SCIENTIFIC REPORTS

OPEN

Relation between colour- and phase changes of a leuco dye-based thermochromic composite

Received: 6 January 2018
Accepted: 20 March 2018
Published online: 03 April 2018

Kristina Bašnec[1], Lidija Slemenik Perše[2,5], Boštjan Šumiga[3], Miroslav Huskić[2], Anton Meden[4], Aleš Hladnik[3], Bojana Boh Podgornik[3] & Marta Klanjšek Gunde[2]

Reversible colour change of leuco dye-based composites is in general closely related to their phase change, thus the two phenomena should occur at around the same temperature and should be influenced similarly. However, spatial confinement of the analysed sample affects the change in colour differently compared to its phase transition and the most pronounced effects can be observed during cooling. The bulk composite is coloured while still liquid and the colour hysteresis does not exhibit a loop. In an open-porous medium the colouration coincides well with the crystallization and the colour hysteresis widens to about 4 °C. Microencapsulated composite exhibits two crystallization processes, one of them taking place at the bulk crystallization temperature and the other one at about 20 °C lower. Under such conditions the composite is coloured just before the onset of the second crystallization, i.e. about 15 °C below crystallization in the bulk, and the corresponding colour hysteresis widens to 18 °C. The two crystallization forms are thermally independent and have the same crystalline structure. These effects should be taken into account when designing future applications where the phase-changing materials are implemented.

Organic thermochromic (TC) materials are applied in a wide range of commercial products such as in colour-changing textiles[1–4], for temperature control of a foldable paper or textile[5] and even for colour-changing wood veneers[6]. In these applications the TC material is used in a spatially confined form. Most frequently, micro-encapsulation is used to produce colour-changing "pigments" suitable for printing inks.

During the last decades, the leuco dye-based TC materials have received substantial attention from both researchers and industry. In these materials, the temperature-induced colour change occurs due to molecular rearrangement of colour formers (leuco dyes) in the presence of a developer and this process is controlled by a phase change of the co-solvent. The molecular mechanisms were thoroughly studied in fully coloured as well as in totally decoloured states, i.e. in solid and liquid states of the composite, respectively[7–14]. However, a leuco dye-based TC composite can solidify without changing its colour, and the colourless solid state can exist within a reasonably wide temperature region[15]. Such a state has not yet been studied in more detail.

The colour change as a function of temperature produces a hysteresis which is very narrow for TC composites and much wider for printing inks where these are microencapsulated to protect the phase-changing material (PCM) from its surrounding[16–19]. The shape of the colour hysteresis provides the first evidence of changes in the TC composite, such as poor fastness against light and high temperatures[18]. To the best of our knowledge, the relationship between the phase- and colour changes has not yet been analysed.

The phase changes of leuco dye-based TC composites are controlled by the applied co-solvent, which can be a long-chain alkyl alcohol, ester, ketone, ether, or acid[1,2]. Such PCMs were extensively investigated to determine the relationship between their structure and energy storage properties in eutectic mixtures for the solid-liquid transition[20–24]. PCMs are commonly used in a microencapsulated form[1,25–30] but this can change their thermal properties when measured in the bulk[31]. In many cases, supercooling lowers crystallization temperature, depending on the type of polymer shell and the size of microcapsules[32–35]. A greatly reduced number of nucleation sites

[1]Radeče Papir Nova, d.o.o., Njivice 7, SI-1433, Radeče, Slovenia. [2]National Institute of Chemistry, Hajdrihova 19, SI-1000, Ljubljana, Slovenia. [3]University of Ljubljana, Faculty of Natural Sciences and Engineering, Aškerčeva cesta 12, SI-1000, Ljubljana, Slovenia. [4]University of Ljubljana, Faculty of Chemistry and Chemical Technology, Večna pot 113, SI-1000, Ljubljana, Slovenia. [5]Present address: University of Ljubljana, Faculty of Mechanical Engineering, Aškerčeva 6, SI-1000, Ljubljana, Slovenia. Correspondence and requests for materials should be addressed to M.K.G. (email: marta.k.gunde@ki.si)

induces an independent crystallization within isolated parts of the material, known as homogeneous nucleation. Different nucleation efficiency in microcapsules of various sizes may result in multiple crystallization peaks[31]. Supercooling of 10 °C and more was investigated during the crystallization of mini-emulsion droplets (immiscible liquid drops of 100–500 nm) of alkanes[36,37]. Mini-emulsions of immiscible polymer blends with a broad size distribution of droplets were shown to have multiple crystallization peaks; a broader size distribution leads to a larger number of peaks[38].

Large effects were also observed in porous media. Crystallization of a fluid in a nanometer-sized porous material resulted in a much lower freezing temperature, i.e. in a more pronounced supercooling effect, which was described as a layer-by-layer crystal growth[39]. Freezing of n-alcohols in mesoporous silicon was obtained at 28 °C lower temperature than in the bulk[40].

The most important research of a TC composite in spatially confined conditions was done for its application as the active core in fibres made by melt coaxial electrospinning. It was shown that the thermal and colouration properties of the active core were only slightly affected in fibres with a diameter of 0.5–2 μm[3], but many changes were found in fibres with a diameter of 1.7–5.7 μm[4]. Multiple solidification peaks observed in dynamic DSC curves were contributed to different diameters of the fibre's core and the change in freezing temperature was linked to possible reactions between the polymer shell and the active core inside the microcapsules. It was also concluded that the phase transition temperature might not be the only parameter governing the colour transition temperature[4].

The above results were a strong motivation for our research. If the colour of leuco dye-based TC composites follows their phase transition temperatures, their colour and phase changes should be equally affected by a spatial micro-arrangement. To analyse this assumption, the same TC composite was studied both in the bulk and in a confined form. Because TC composites can only seldom be applied in the bulk, the obtained results should be important for a design of the functional properties of the final application.

Results and Discussion

Colour properties. The shape of the hysteresis was described by the loop width and four characteristic temperatures, describing the onset (T_1 and T_3) and termination (T_2 and T_4) of the TC effect: discolouration at heating (T_1 and T_2) and colouration at cooling (T_3 and T_4), respectively (Fig. S1, Supplementary information).

The temperature-dependent colour and thermal properties of the three forms of the TC composite are shown in Fig. 1 and the data describing the colour hysteresis in Table 1. The same heating and cooling rates (5 °C/min and 10 °C/min, respectively) were used to enable comparison between the two measurements.

In the bulk state (C6), the composite discolours before the melting is completed (transition A) but it re-colours well above the freezing point (transition B). This confirms that colouration/discolouration of a TC composite may not follow the phase changes[15], however, a coloured liquid is formed before solidification and colourless solid before melting. The corresponding colour hysteresis possesses an unusual shape where the cooling and heating curves intersect. This is in agreement with our previous research - TC composites have a very narrow colour hysteresis and in some cases the two curves may also cross each other[41]. When the composite is inside the paper (pC6), transitions A and B remain practically unaffected, but the colour hysteresis broadens to about 4 °C and becomes less steep than in the bulk. Moreover, discolouration of the sample at heating and re-colouration at cooling coincide well with the temperatures where melting (A) and crystallization (B) processes are completed. The μC6 sample shows two phase transitions at cooling, one at crystallization of its bulk form (B) and another one at much lower temperatures (C) and the colour hysteresis is very broad (~18 °C). This sample discolours at higher temperatures than in the bulk form (C6) and inside the paper (pC6), but still at about 6 °C below the temperature at which the active core inside microcapsules completely melts. Re-colouration of the sample occurs at considerably lower temperatures than in the other two forms and completes just before the onset of the transition C.

Discolouration upon heating starts at virtually the same temperature in all three samples (T_1) but completes at a higher temperature (T_2) in the paper (pC6) and especially in the microcapsules (μC6). A stronger influence of the spatial conditions of the TC composite on its colouration and phase changes was recorded at cooling, the most pronounced in the microencapsulated form. A direct comparison of the thermal and colouration properties of the analysed TC composite is shown in Fig. S2 (Supplementary information).

Thermal properties. A slow DSC experiment (Fig. 2a) resolved the details obscured by the rapid scanning used to obtain the colorimetric measurements (Fig. 1). The results were compared with those for the ML co-solvent in the same three forms (Fig. 2b). The corresponding phase change temperatures and transition enthalpies are given in Table 2. The mass of the host material (paper and microcapsule's shells) was not taken into account, therefore thermograms were normalized according to the melting peak (A) and transition enthalpies can be compared only among samples with the same holding material.

DSC thermograms of the TC composite and of the applied co-solvent show the same features with systematically larger transition enthalpies with the latter, thus these transitions are driven by the co-solvent. Two (or even three) transition peaks were resolved at bulk crystallization (transition B), lower in μML and higher in μC6. The μML sample shows peaks also between transitions B and C where practically no features were observed in the μC6 sample (Fig. S3, Supplementary information).

The supercooling effect of transition B is very small, about 1 °C for the composite and about 2 °C for the co-solvent. Thus, the spatial separation of the PCM is not critical and transition B can be regarded as having a bulk nature. The size effect of the microcapsules is discussed later in the article.

To understand the measured crystallisation properties, two questions have to be answered – first, are the transitions B and C thermally related and, second, if the two transitions lead to the same crystal structure (i.e. to the same crystalline polymorph). The first question was addressed by combining static and dynamic DSC measurements and the second one by performing powder XRD measurements.

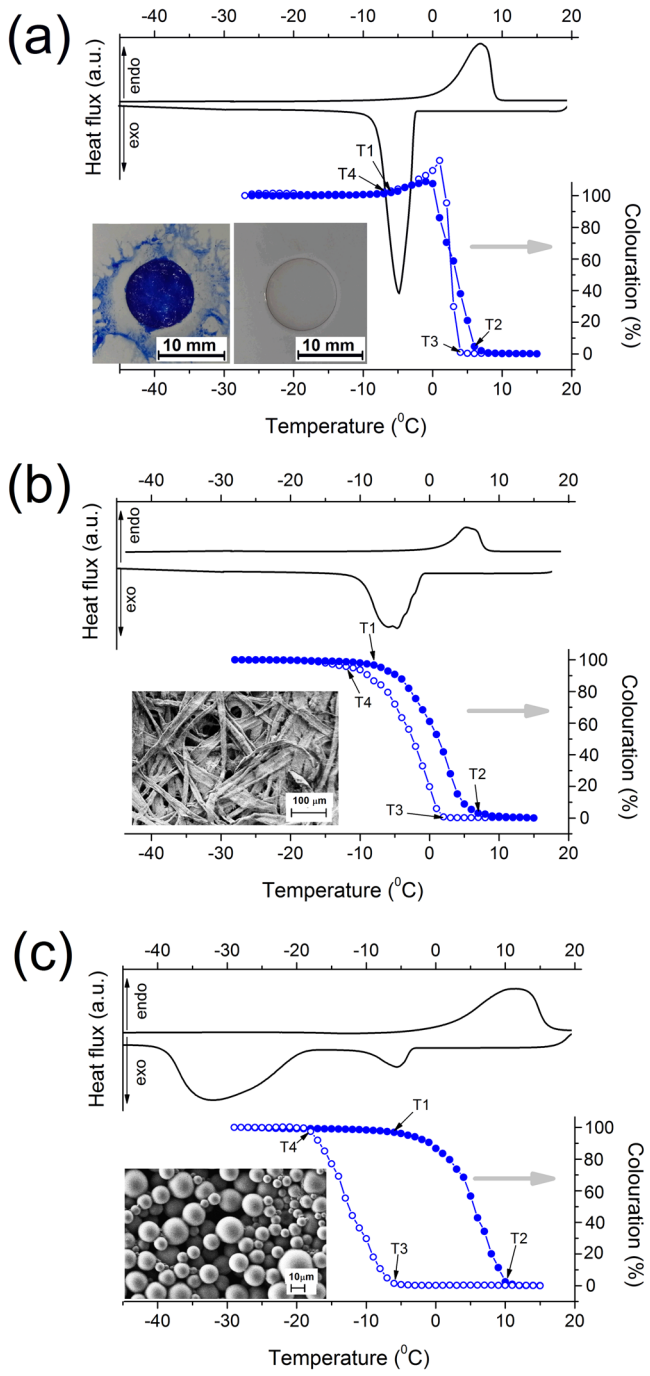

Figure 1. Thermal (DSC, black curve) and colorimetric properties (blue curve with circles) of the (**a**) TC composite in the bulk, (**b**) inside the chromatographic paper and (**c**) in microcapsules. Heating and cooling rates of 5 °C/min and 10 °C/min, respectively, were used for both measurements. Pictures of the corresponding holders are included. The bulk composite is shown in the fully coloured and totally discoloured states (**a**).

Sample	Width (°C)	T_1 (°C)	T_2 (°C)	T_3 (°C)	T_4 (°C)
C6	—	−7	6	4	−6
pC6	4	−8	7	2	−12
µC6	18	−6	10	−6	−18

Table 1. The onset (T_1 and T_3) and termination (T_2 and T_4) temperatures of the TC effect - discolouration at heating (T_1 and T_2) and colouration at cooling (T_3 and T_4), respectively, for the colour hysteresis of the C6, pC6, and µC6 samples. See also Figs 1, S1 and S2.

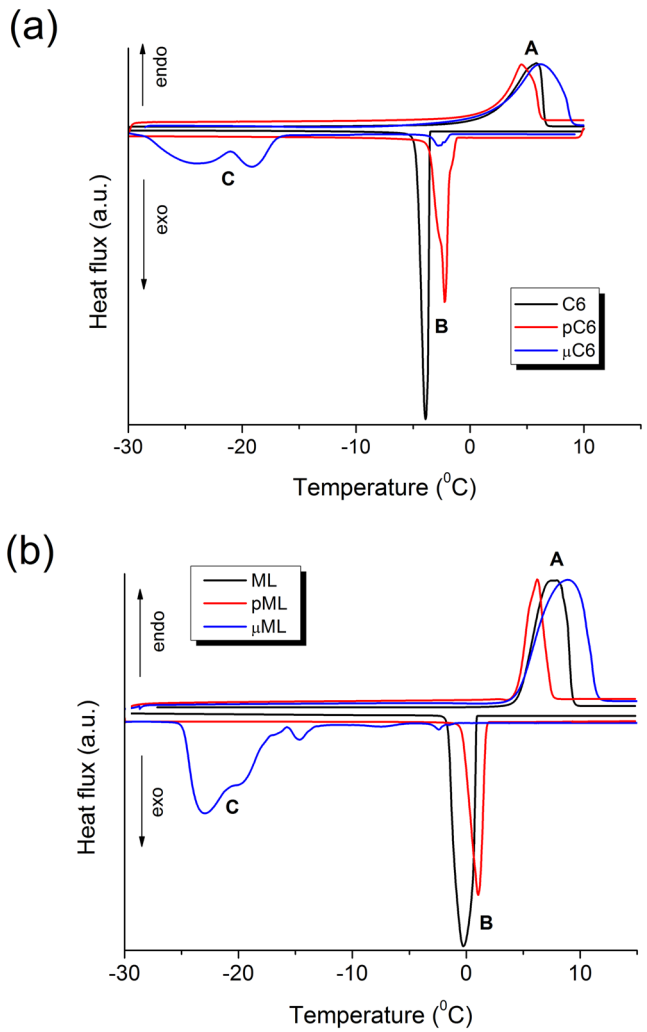

Figure 2. DSC thermograms of (**a**) the TC composite (C6, pC6, and µC6), and (**b**) the applied co-solvent (ML, pML, µML). The heat fluxes were normalized according to the melting peak (transition A). Both heating and cooling rates were 2 °C/min.

Sample	Transition A		Transition B		Transition C	
	T_{pc} (°C)	ΔH (J/g)	T_{pc} (°C)	ΔH (J/g)	T_{pc} (°C)	ΔH (J/g)
C6	5.5	150	−2.4	−162	—	—
pC6	4.5	27	−2.0	−28	—	—
µC6	6.1	115	−2.2, −2.7	−5	−19.0, −24.0	−94
ML	8.0	530	1.0	−536	—	—
pML	6.3	33	0.6	−32	—	—
µML	8.7	135	−1.5, −2.4	−1	−14.6, −16.6, −20.0, −22.9	111

Table 2. The phase-change temperature (T_{pc}) and the enthalpy (ΔH) of transitions A, B, and C of the analysed materials in bulk (C6, ML), inside the chromatographic paper (pC6, pML) and in microcapsules (µC6, µML). The temperatures of all resolved maxima are given for multiple peaks, while ΔH is for the entire transition. The mass of the paper and of the microcapsules' shell was not taken into account, therefore only comparisons between samples with the same host material are reasonable.

The crystallization properties of the microencapsulated samples were analysed by applying a 20 minute isothermal regime between transitions B and C, i.e. at −10 °C (Fig. 3 and Table 3). When a 20 min isothermal DSC was used after cooling to −10 °C followed by the samples' heating back to 15 °C, the melting enthalpy (transition A) was found to correspond reasonably well with the crystallization one (transition B). When after 20 min isothermal DSC at −10 °C the sample was cooled down to −50 °C, the peaks at transition C were similar to

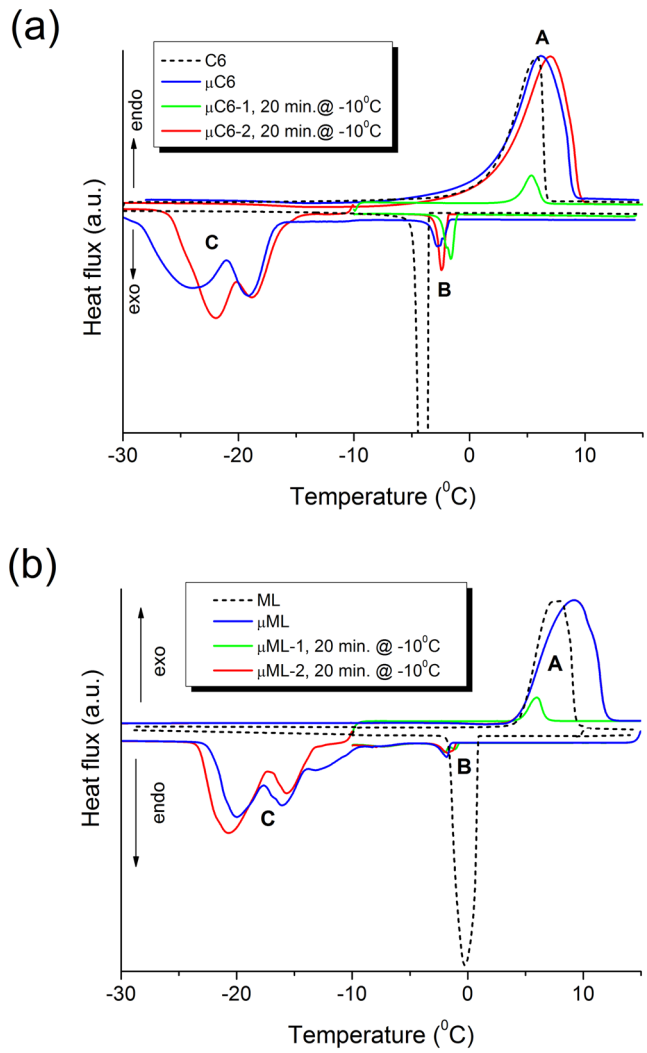

Figure 3. DSC thermograms of (**a**) the composite and (**b**) the co-solvent in the bulk (C6, ML) and microencapsulated forms (μC6, μML). Green curve: 20 min isothermal DSC was used after cooling to −10 °C, followed by heating. Blue curve: after 20 min isothermal DSC taken at −10 °C, the dynamic regime continued to −50 °C, followed by heating. Both heating and cooling rates in the dynamic regime were 2 °C/min.

Sample	Transition A		Transition B		Transition C	
	T_{pc} (°C)	ΔH (J/g)	T_{pc} (°C)	ΔH (J/g)	T_{pc} (°C)	ΔH (J/g)
μML	9.0	142	−1,8	−3	−8.2, −13.1, −16.0, −19.9	−125
μML-1	6.0	8	−1.1, −1.9, −7.3	−4	—	—
μML-2	9.1	142	−1.7	−3	−15.6, −20.6	−121.0
μC6	6.1	116	−2.8	−5	−19.0, −23.9	−93.6
μC6-1	5.3	7	−1.6, −1.9	−6	—	—
μC6-2	6.9	124	−2.3	−6	−18.8, −21.9	−105

Table 3. The phase change temperature (T_{pc}) and the enthalpy (ΔH) of transitions A, B, and C measured for microencapsulated materials in dynamic regime over the entire temperature region (μML, μC6), using 20 min isothermal DSC at −10 °C in the −10 °C to 15 °C temperature region (μML-1, μC6-1) and in the entire temperature region with 20 min isothermal DSC at −10 °C (μML-2, μC6-2). The temperatures of all resolved maxima are given for multiple peaks while ΔH is for the entire transition.

those when only a dynamic DSC was applied. Moreover, almost an identical curve was produced upon heating (compare blue and red curves in Fig. 3). The 20 minutes isothermal regime used at −10 °C caused a negligible crystallization, thus the transition A remained practically unaffected when cooling was stopped. Similar results

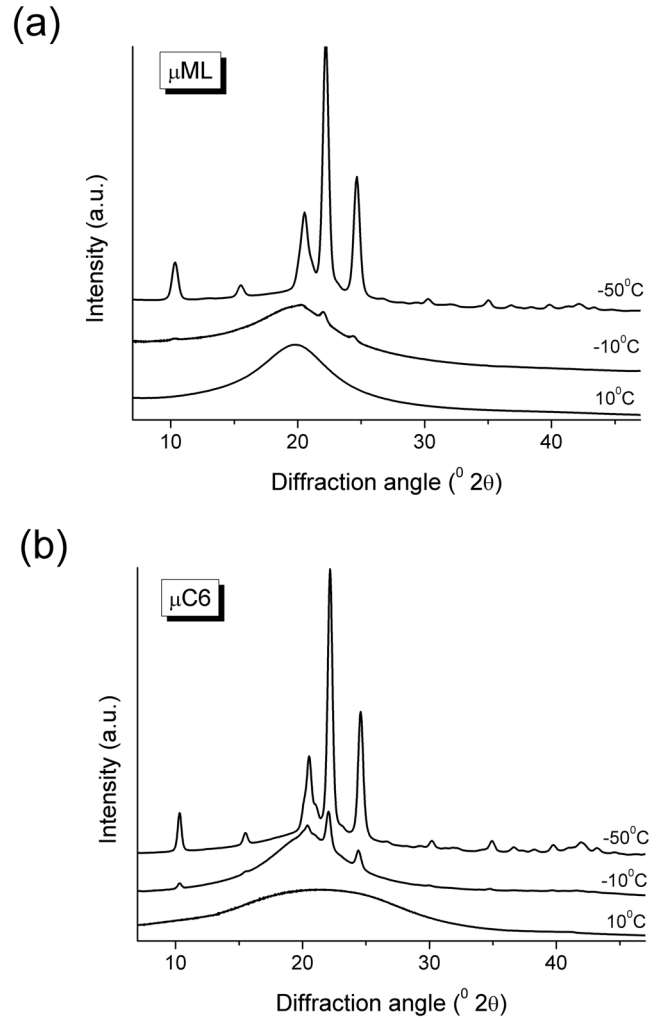

Figure 4. Powder XRD patterns of (**a**) μML and (**b**) μC6 samples after cooling to 10 °C, −10 °C, and −50 °C.

were obtained for the TC composite and for the co-solvent. It is therefore safe to conclude that the transitions B and C are thermally independent.

Crystalline phase. The crystalline phase, resulting from the transitions B and C was checked by powder XRD of the samples μML and μC6 cooled down to 10 °C, −10 °C and −50 °C. At 10 °C, both samples are amorphous, as expected – according to the DSC results, they are still liquid at this temperature. However, at −10 °C and −50 °C the diffraction patterns show the appearance of peaks, confirming that for both samples, the thermal effects are due to crystallization. The appearance of diffraction peaks at the same diffraction angles and having the same intensity ratios clearly indicates that the crystalline phase is apparently the same in all cases (both samples and both temperatures, just its amount is larger at −50 °C in both samples, see Fig. 4). We can conclude that the presence of the dye does not affect the crystallization to the extent that another polymorph of ML or co-crystal would crystallize. It has to be noted that no crystal structure data for ML are available so that structure-related discussion of the powder patterns is neither possible nor needed for the purpose of this work.

Spatial confinement effect. The microencapsulated samples have a broad size distribution, ranging from 1.6 to 25.4 μm with the median 9.4 μm for μC6 (Fig. 5) and similar for μML (Fig. S4a). The samples have the same thickness as microcapsules' shell (Table 4).

To investigate the influence of the microcapsules' size on the colorimetric and thermal properties, the μC6 and μML dispersions were gravimetrically separated into fractions with smaller (μC6-s, μML-s) and larger microcapsules (μC6-l, μML-l), respectively; see Figs 6a,b, and S4a,b. The size of the microcapsules in the obtained samples is given in Table 4 and the corresponding DSC thermograms are shown in Figs 6c and S4d (Supplementary information) with the corresponding thermal data displayed in Table 5.

The transition B does not appear in DSC thermograms for smaller microcapsules (<11 μm, μC6-s and μML-s), but only for larger ones. The transition C consists of multiple peaks (Figs 6c, S4), which is typical for crystallization in mini-emulsion droplets[36–38].

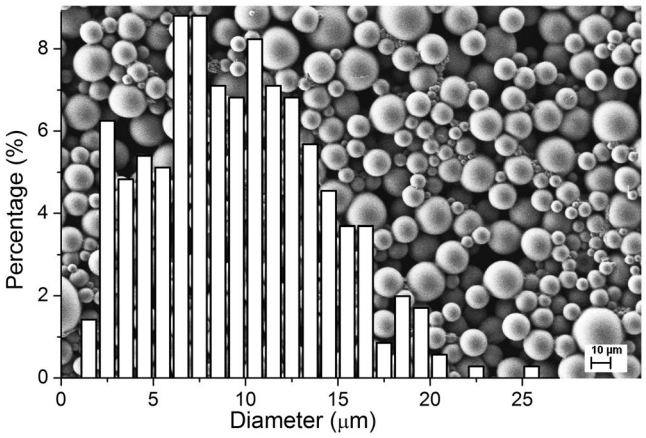

Figure 5. The size distribution and typical SEM micrograph of the μC6 sample.

Sample	Diameter (μm)			Shell thickness (nm)
	Mean	Median	Range (min < > max)	
μC6	9.6	9.4	1.6 < > 25.4	119 ± 5
μC6-s	8.4	8.2	3.7 < > 15.3	
μC6-l	18.4	18.4	12.9 < > 25.1	
μML	9.8	9.2	1.6 < > 24.0	118 ± 5
μML-s	4.3	3.9	1.1 < > 11.3	
μML-l	16.8	16.5	9.6 < > 22.8	

Table 4. Diameter (mean, median, and range of the size distribution) and shell thickness for the prepared microcapsules (μC6, μML) and for smaller (μC6-s, μML-s) and larger microcapsules (μC6-l, μML-l). The shell thickness was measured on the SEM micrographs where the capsules were cut with a scalpel.

Thermal properties of the TC composite and of the applied co-solvent are very similar, leading to the conclusion that the phase changes of the TC composite are predominantly driven by the co-solvent while the other two components (leuco dye and developer) have only a minor influence. However, the colouration-discolouration ability is subject to the dye-developer interactions in the phase-changing co-solvent, and discolouration requires the interaction between a developer and a co-solvent. This interaction might strongly depend on the host material, especially on its morphology and the latter can be of considerable importance. For a deeper understanding of this topic, spectroscopic investigations would be necessary; however, the contribution of the host material will inevitably obscure the properties of the composite. In addition, good temperature stability during measurements must be assured. We will try to do some progress in this direction in our future work.

Conclusions

Colour changes of the analysed leuco dye-based TC composite become loosely related to its phase transitions when the material is restricted within micrometer dimensions of a holding medium. The strongest effects are observed in microcapsules when cooling where their colour changes well before crystallization and the corresponding hysteresis is extremely wide. Two thermally independent exothermic transitions with the same crystalline structure were found – a weak one at bulk crystallization temperature and a much stronger one at a more than 15 °C lower temperature. Apparently, the low-temperature crystallization shifts the colouration of the microencapsulated composite to much lower temperatures, but not all the way to the phase change temperature. On the other hand, the open nature of the porous structure with narrower particle sizes than the smallest microcapsules shows only the bulk crystallization and the colour changes follow the phase transitions reasonably well. Here, the colour hysteresis exhibits a standard loop shape.

To the best of our knowledge, this is the first report of the influence of spatial confinement on the colour- and phase changes of a leuco dye-based TC composite. Both phenomena depend on the conditions in which the PCM is captured, but are only loosely related to each other. The results presented in the paper are important for designing different applications where such materials are used.

Methods

Crystal violet lactone leuco dye (CVL, >95%, Tokyo Chemical Industry), benzyl 4-hydroxybenzoate (B4HB, >99%, Tokyo Chemical Industry) and methyl laurate (ML, 96%, Acros OrganicsTM, Fisher Scientific) were used as received. The TC composite (C6) was prepared by dissolving B4HB and CVL in the ML co-solvent in molar ratio CVL:B4HB:ML = 0.5:6:100.

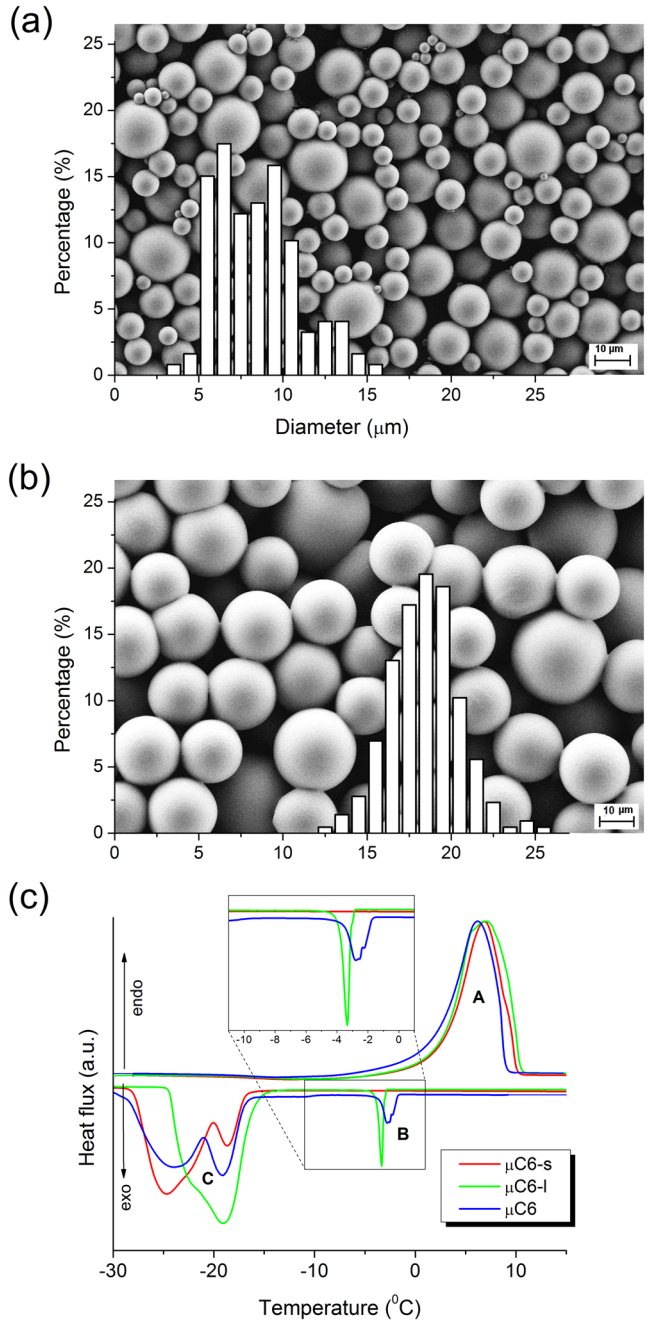

Figure 6. SEM micrographs of (**a**) μC6-s and (**b**) μC6-l samples with the corresponding particle size distributions. (**c**) DSC thermograms (2 °C/min) of μC6 (blue) and of its fractions μC6-s (red) and μC6-l (green), normalized according to the melting peak (transition A).

The chromatography paper No. 232-674-98 (85 g/m², 2-4 μm pore size, Machery-Nagel GmbH & Co. KG) was used to spread the material into the porous paper (pC6, pML).

Microencapsulation (μC6, μML) was done by *in situ* polymerization of amino-aldehyde prepolymers[42,43]. All materials for the microcapsule shell originated from the continuous aqueous phase of the oil-in water emulsion. A modifying agent was added to enable polymerization of the aminoaldehyde precondensate only at the surface of the emulsified microcapsule cores. Under controlled polymerization conditions (pH, temperature) total mass of the shell material precipitated and was distributed evenly over the surface of droplets in the emulsion. This resulted in a uniform microcapsule shell thickness, regardless of the microcapsule size. Such result was also reported in previous studies[44,45].

The size distribution of microcapsules was obtained by image analysis of SEM micrographs (Karl Zeiss Supra 35 C) using ImageJ image processing software with suitable numerical procedures[46].

Temperature-dependent colour of the C6 was measured inside a cylindrical groove (11.2 mm diameter, 0.3 mm depth) in the 2.9 mm thick white-coated copper plate. The colour of the μC6 was measured on a thin

sample	Transition A		Transition B		Transition C	
	T_{pc} (°C)	ΔH (J/g)	T_{pc} (°C)	ΔH (J/g)	T_{pc} (°C)	ΔH (J/g)
µML	9.0	142	−1,8	−3	−8.2, −13.1, −16.0, −19.9	−125
µML-s	7.7	155	—	—	−14.5, −16.2, −19.7, −22.5	−134
µML-l	7.4	176	−1.9	−3	−14.4,−21.9	−141
µC6	6.1	115	−2.8	−5	−19.0, −23.9	−94
µC6-s	6.7	152	—	—	−18.6, −24.6	−139
µC6-l	6.8	165	−3.3	−7	−18.9, −22.0	−140

Table 5. The phase change temperature (T_{pc}) and the enthalpy (ΔH) of transitions A, B, and C measured for microencapsulated ML and C6 materials in the as-prepared forms (µML, µC6) and after separation into samples with smaller (µML-s, µC6-s) and larger particle size (µML-l, µC6-l). The temperatures of all resolved maxima are given for multiple peaks while ΔH is for the entire transition.

layer of microcapsules prepared over a white paper using the Film-Applicator (Byk Additives&Instruments) with 200 µm clearance gap and dried at room temperature. All samples were cooled by dry ice (−78.5 °C) down to −30 °C and heated on a laboratory table at room temperature, producing cooling- and heating rates of about 10 °C/min and 5 °C/min, respectively. Temperature of the sample surface was measured by Ni Cr-Ni thermocouple connected to IR thermometer (Fluke 561). Colour of the samples was measured by the i1 Pro spectrometer (X-Rite, USA). The CIELAB colour values with D50 illuminant and 2° standard colorimetric observer were calculated by KeyWizzard software[47]. The colour change was expressed by the CIE colour difference ΔE_{ab}* with respect to the highest measured temperature and normalized according to the totally coloured state taken at the lowest temperature.

Thermal properties were analysed by differential scanning calorimetry (DSC) using Mettler Toledo DSC1 apparatus at heating/cooling rates of 2 °C/min, 5 °C/min, and 10 °C/min from −50 °C to 15 °C. For this purpose, the water dispersions of microcapsules were dried at room temperature.

The XRD patterns were collected on the Rigaku SuperNova diffractometer, equipped with Atlas CCD detector, using CuKα radiation and the Powder power tool within the CrysalisPro data collection software (version 171.37.34t). The cooling of the samples was done using an Oxford Instruments CryoJet device.

References

1. Aitken, D., Burkinshaw, S. M., Griffiths, J. & Towns, A. D. Textile applications of thermochromic systems. *Rev. Prog. Coloration* **26**, 1–8 (1996).
2. White, M. A. & LeBlanc, M. Thermochromism in Commercial Products. *J. Chem. Educat.* **76**, 1201–1205 (1999).
3. Li, F. *et al*. Thermochromic Core-Shell Nanofibers Fabricated by melt Coaxial Electrospinning. *J. Appl. Polym. Sci.* **112**, 269–274 (2009).
4. Malherbe, I., Sanderson, R. D. & Smit, E. Reversibly thermo-chromic microfibres by coaxial electrospinning. *Polymer* **51**, 5037–5043 (2010).
5. Busuioc, C., Evanghelidis, A., Galatanu, A. & Enculescu, I. Direct and contactless electrical control of temperature of paper and textile foldable substrates using electrospun metallic-web transparent electrodes. *Sci. Rep.* **6**, 34584, https://doi.org/10.1038/srep34584 (2016).
6. Zhu, X., Liu, Y., Dong, N. & Li, Z. Fabrication and characterization of reversible thermochromic wood veneers. *Sci. Rep.* **7**, 16933, https://doi.org/10.1038/s41598-017-17238-9 (2017).
7. Burkinshaw, S. M., Griffiths, J. & Towns, A. D. Reversibly thermochromic systems based on pH-sensitive spirolactone-derived functional dyes. *J. Mater. Chem.* **8**, 2677–2683 (1998).
8. MacLaren, D. C. & White, M. A. Dye–developer interactions in the crystal violet lactone–lauryl gallate binary system: implications for thermochromism. *J. Mater. Chem.* **13**, 1695–1700 (2003).
9. MacLaren, D. C. & White, M. A. Competition between dye–developer and solvent–developer interactions in a reversible thermochromic system. *J. Mater. Chem.* **13**, 1701–1704 (2003).
10. Luthern, J. & Peredes, A. Determination of the stoichiometry of a thermochromic color complex via the method of continuous variation. *J. Mater. Sci. Lett.* **22**, 881–884 (2003).
11. Zhu, C. F. & Wu, A. B. Studies on the synthesis and thermo-chromic properties of crystal violet lactone and its reversible thermochromic complexes. *Thermochim. Acta* **425**, 7–12 (2005).
12. MacLaren, D. C. & White, M. A. Design rules for reversible thermochromic mixtures. *J. Mater. Sci.* **40**, 669–676 (2005).
13. Tang, H., MacLaren, D. C. & White, M. A. New insights concerning the mechanism of reversible thermochromic mixtures. *Can. J. Chem.* **88**, 1063–1070 (2010).
14. Borque, A. N. & White, M. A. Control of thermochromic behaviour in crystal violet lactone (CVL)/alkyl gallate/alcohol ternary mixtures. *Can. J. Chem.* **93**, 22–31 (2015).
15. Hajzeri, M., Bašnec, K., Bele, M. & Klanjšek Gunde, M. Influence of developer on structural, optical and thermal properties of a benzofluoran-based thermochromic composite. *Dyes Pigm.* **113**, 754–762 (2015).
16. Kulčar, R., Friškovec, M., Hauptman, N., Vesel, A. & Klanjšek Gunde, M. Colorimetric properties of reversible thermochromic printing inks. *Dyes Pigm.* **86**, 271–277 (2010).
17. Kulčar, R., Friškovec, M., Klanjšek Gunde, M. & Knešaurek, N. Dynamic colorimetric properties of mixed thermochromic printing inks. *Color. Technol.* **127**, 411–417 (2011).
18. Friškovec, M., Kulčar, R. & Klanjšek Gunde, M. Light fastness and high-temperature stability of thermochromic printing inks. *Color. Technol.* **129**, 214–222 (2013).
19. Panák, O., Držková, M. & Kaplanová, M. Insight into the evaluation of colour changes of leuco dye based thermochromic systems as a function of temperature. *Dyes & Pigm.* **120**, 279–287 (2015).
20. Zhang, J. J., Zhang, J. L., He, S. M., Wu, K. Z. & Liu, X. D. Thermal studies on the solid-liquid phase transition in binary systems of fatty acids. *Thermochim. Acta* **369**, 157–160 (2001).

21. Ventolà, L. *et al*. Solid state equilibrium in the n-alkanols family: the stability of binary mixed samples. *Phys. Chem. Chem. Phys.* **5**, 947–752 (2003).
22. Ventolà, L., Calvet, T., Cuevas-Diarte, M. A., Oonk, H. A. J. & Mondieig, D. Solid–solid and solid–liquid equilibria in the n-alkanols family: $C_{18}H_{37}OH$–$C_{20}H_{41}OH$ system. *Phys. Chem. Chem. Phys.* **6**, 3726–3731 (2004).
23. Zuo, J., Li, W. & Weng, L. Thermal performance of caprylic acid/1-dodecanol eutectic mixture as phase change materials (PCM). *Energy Build.* **43**, 207–210 (2011).
24. Liston, L. C. *et al*. Binary mixtures of fatty acid methyl esters as phase change materials for low temperature applications. *Appl. Therm. Engn.* **96**, 501–507 (2016).
25. Nelson, G. Application of microencapsulation in textiles. *Int. J. Pharmaceuticals* **242**, 55–62 (2002).
26. Guo, X., Cao, J., Peng, Y. & Liu, R. Incorporation of microencapsulated dodecanol into wood flour/high density polyethylene composite as a phase change material for thermal energy storage. *Materials and Design* **89**, 1325–1334 (2016).
27. Li, W. *et al*. Design, controlled fabrication and characterization of narrow-disperse macrocapsules containing Micro/nanoPCMs. *Materials and Design* **99**, 225–234 (2016).
28. Meng, F., Wang, S., Liu, H., Xu, X. & Ma, H. Microencapsulation of oxalic acid (OA) via coacervation induced by polydimethylsiloxane (PDMS) for the sustained release performance. *Materials and Design* **116**, 31–41 (2017).
29. Shams, T., Parhizkar, M., Illangakoon, U. E., Orlu, M. & Edirisinghe, M. Core/shell microencapsulation of indomethacin/paracetamol by co-axial electrohydrodynamic atomization. *Materials and Design* **136**, 204–213 (2017).
30. Nomura, T., Zhu, C., Sheng, N., Saito, G. & Akiyama, T. Microencapsulation of Metal-based Phase Change Material for High-temperature Thermal Energy Storage. *Sci. Rep.* **5**, 9117, https://doi.org/10.1038/srep09117 (2015).
31. Chaiyasat, P., Noppalit, S., Okubo, M. & Chaiyasat, A. Do encapsulated heat storage materials really retain their original thermal properties? *Phys. Chem. Chem. Phys.* **17**, 1053–1059 (2015).
32. Zhang, Y. X., Fan, Y. F., Tao, X. M. & Yick, K. L. Crystallization and prevention of supercooling of microencapsulated n-alkanes. *J. Coll. Interf. Sci.* **281**, 299–306 (2005).
33. Zhang, S. & Niu, J. Experimental investigation of effects of supercooling on microencapsulated phase-change material (MPCM) slurry thermal storage capacities. *Sol. En. Mat. Sol. Cells* **94**, 1038–1048 (2010).
34. Tang, X., Li, W., Zhang, X. & Shi, H. Fabrication and characterization of microencapsulated phase change material with low supercooling for thermal energy storage. *Energy* **68**, 160–166 (2014).
35. Cao, F. & Yang, B. Supercooling suppression of microencapsulated phase change materials by optimizing shell composition and structure. *Appl. Energy* **113**, 1512–1518 (2014).
36. Montenegro, R., Antonietti, M., Mastai, Y. & Landfester, K. Crystallization in Miniemulsion Droplets. *J. Phys. Chem. B* **107**, 5088–5094 (2003).
37. Montenegro, R. & Landfester, K. Metastable and Stable Morphologies during Crystallization of Alkanes in Miniemulsion Droplets. *Langmuir* **19**, 5996–6003 (2003).
38. Tol, R. T., Mathot, V. B. F. & Groeninckx, G. Confined crystallization phenomena in immiscible polymer blends with dispersed micro- and nanometer sized PA6 droplets, part 2: reactively compatibilized PS/PA6 and (PPE/PS)/PA6 blends. *Polymer* **46**, 369–382 (2005).
39. Alba-Simionesco, C. *et al*. Effects of confinement on freezing and melting. *J. Phys.: Condens. Matter.* **18**, R15–68 (2006).
40. Berwanger, R., Schumacher, C., Huber, P. & Pelster, R. Size-dependent freezing of n-alcohols in silicon nanochannels, Eur. Phys. J. *Special Topics* **189**, 239–249 (2010).
41. Panák, O., Hauptman, N., Klanjšek Gunde, M. & Kaplanová, M. Colorimetric characterization of thermochromic composites with different molar ratios of components. *JPMTR* **1**, 113–120 (2012).
42. Šumiga, B. *et al*. B, Production of Melamine-Formaldehyde PCM Microcapsules with Ammonia Scavenger used for Residual Formaldehyde Reduction. *Acta Chim. Slov.* **58**, 14–25 (2011).
43. Boh, B., Knez, E. & Starešinič, M. Microencapsulation of higher hydrocarbon phase change materials by *in situ* polymerization. *Journal of microencapsulation* **22**, 715–735 (2005).
44. Pretzl, M. *et al*. Formation and mechanical characterization of aminoplast core/shell microcapsules. *ACS applied materials & interfaces* **4**, 2940–2948 (2012).
45. Yuan, Y. C., Rong, M. Z. & Zhang, M. Q. Preparation and characterization of microencapsulated polythiol. *Polymer* **49**, 2531–2541 (2008).
46. Gonzalez, R. C., Woods, R. E. RE: Digital Image Processing. 3rd Ed. Prentice-Hall: Upper Saddle River, New Jersey 2008.
47. J. Shanda, CIE colorimetry. In: Shanda J, editor. Colorimetry; understanding the CIE system. Hoboken: Wiley, p. 25–78 (2007).

Acknowledgements

The financial support from the state budget by the Slovenian Research Agency (Project No. L2-5571) and the EN-FIST Centre of Excellence, Slovenia for use of the Supernova diffractometer are acknowledged.

Author Contributions

K.B. made the formulation and preparation of the active material, L.S.P. contributed with colorimetric and SEM measurements, B.Š. and B.B.P. made microencapsulation of the composite, M.H. provided DSC analysis and size separation of microcapsules, A.M. made XRD measurements and explanations, A.H. provided the particle size distribution analysis of SEM micrographs, and M.K.G. lead the entire research and wrote the article.

Additional Information

Supplementary information accompanies this paper at https://doi.org/10.1038/s41598-018-23789-2.

Competing Interests: The authors declare no competing interests.

Publisher's note: Springer Nature remains neutral with regard to jurisdictional claims in published maps and institutional affiliations.